Triggered cagedSTORM microscopy

PÉTER BÍRÓ,[1,*] TIBOR NOVÁK,[1] ELVIRA CZVIK,[1] JÓZSEF MIHÁLY,[2,3] SZILÁRD SZIKORA,[2] SEBASTIAN VAN DE LINDE,[4] AND MIKLÓS ERDÉLYI[1]

[1]*Department of Optics and Quantum Electronics, University of Szeged, Dóm tér 9, Szeged 6720, Hungary*
[2]*Institute of Genetics, HUN-REN Biological Research Centre Szeged, Temesvári körút 62, Szeged 6726, Hungary*
[3]*Department of Genetics, University of Szeged, Közép fasor 52, Szeged 6726, Hungary*
[4]*Department of Physics, SUPA, University of Strathclyde, Glasgow G4 0NG, Scotland, United Kingdom*
*biro.peter@szte.hu

Abstract: In standard SMLM methods, the photoswitching of single fluorescent molecules and the data acquisition processes are independent, which leads to the detection of single molecule blinking events on several consecutive frames. This mismatch results in several data points with reduced localization precision, and it also increases the possibilities of overlapping. Here we discuss how the synchronization of the fluorophores' ON state to the camera exposure time increases the average intensity of the captured point spread functions and hence improves the localization precision. Simulations and theoretical results show that such synchronization leads to fewer localizations with 15% higher sum signal on average, while reducing the probability of overlaps by 10%.

1. Introduction

Conventional optical microscopes have a spatial resolution limited by the diffraction of light. Different superresolution methods have been developed to overcome this constraint, such as structured illumination microscopy (SIM) [1], stimulated emission depletion (STED) [2] and single molecule localization microscopy (SMLM) [3]. SMLM techniques including (fluorescent) photoactivation localization microscopy (fPALM) [4,5], (direct) stochastic optical reconstruction microscopy (dSTORM) [6,7], points accumulation for imaging in nanoscale topography (PAINT) [8], ground state depletion microscopy followed by individual molecule return (GSDIM) [9] and minimal photon fluxes (MINFLUX) [10] are some of the most powerful superresolution methods in biological studies [11]. In these techniques, the positions of individual molecules are determined by curve fitting to their images referred to as Point Spread Functions (PSF). The determined positions and other parameters are used for generating the superresolution image and the quantitative post processing analysis. One important parameter of these fits is their localization precision, which strongly depends on the number of the collected photons [12]. The acquisition time of the detector is matched to the fluorescent ON state lifetime, and is typically in the range of 5 to 100 ms [13]. Since the exposures of the camera sequentially follow one another, and the individual blinking events start stochastically, one such event is more likely to be captured on multiple consecutive camera frames resulting in several, less accurate localizations [14]. This could lead to an overestimation of the number of emitters, which is typically handled by grouping localizations within a given space and time window [15–22]. The disadvantage of grouping such localizations is that it can link different fluorophores to each other, especially on high-density datasets [23]. Merging localizations of different fluorophores can be avoided by capturing a blinking event on fewer frames. This can be achieved by increasing the excitation laser intensity, thus shortening the ON state lifetime of the fluorophore below the exposure time while potentially risking additional activation through the readout-wavelength. This is generally not desirable

as it increases the duty cycle and thus limits the achievable image resolution according to the Nyquist sampling criterion [24–27]. Here we aim to match the fluorescent ON state lifetime to the exposure time by the controlled activation of the fluorophores triggered by the detector. During caged or PALM-like measurements, the reduced or inactive fluorescent molecules can be reactivated with UV illumination [28–31]. Modulated and synchronized excitation, activation and reactivation have been applied in several SMLM techniques. In the PALM and fPALM methods, under continuous excitation short laser pulses switch on the fluorescent proteins. The activation laser can be modulated via a motorized filter wheel [5] or by means of a galvanometer controlled by a computer and synchronized to the EMCCD camera [4]. In single and multicolor STORM methods the lasers can also be synchronized with the camera [6,32] enabling an effective, multicolor, 3D superresolution imaging of brain tissues [33]. The question is, how much image enhancement can be achieved with a perfectly matched system?

Statistical calculations and TestSTORM [34,35] simulations were performed for the evaluation of advantages and limitations of the triggered activation approach. The derived statistical model was used to calculate the frame duration and the overlapping probabilities, the average time durations and the intensity of blinking events. In addition to the statistical analysis of individual molecule blinking, TestSTORM simulations were applied to visualize the tangible quality enhancement of 2D images. Preliminary experimental results show an increase in the mean sum signal of the captured point spread functions allowing stricter filters on the localization data, and hence a more accurate quantitative evaluation.

2. Theoretical results

In the triggered approach, instead of illuminating the sample continuously with the activation laser (resulting in spontaneous blinking – spontaneous approach, Fig. 1(A)), we switch on the fluorophores with a short reactivation laser pulse at the beginning of an exposure (Fig. 1(B)). This causes the blinking events to start at the beginning of an exposure, increasing the number of blinking events that are captured on a single frame (and the number of exposures without any localization). Here we discuss the case where only UV illumination activates the fluorophores.

2.1. Statistical calculations

2.1.1. Frame duration probabilities

Let us select a blinking event starting on a given frame. The starting time follows a uniform distribution within the frame time, thus the probability of the blinking event to start in the $[t_{s1}, t_{s2}]$ time interval ($0 \leq t_{s1} \leq t_{s2} \leq T$) and to end in the $[t_{l1}, t_{l2}]$ interval (relative to the start of the blinking event) is

$$P(s1 : s2, l1 : l2) = \int_{t_{s1}}^{t_{s2}} \frac{1}{T} \int_{t_{l1}}^{t_{l2}} \frac{1}{\tau} e^{-t_l/\tau} dt_l dt_s, \tag{1}$$

where T is the exposure time, and τ is the expected lifetime of the ON state assuming a single exponential distribution. By restricting the length of the blinking event between frames (so that the blinking event would last until the desired frame, but end before the next exposure), one can calculate the frame duration probabilities. Due to the lower bound of the inner integral, the single frame case ($N = 1$, where $0 \leq t_l \leq T - t_s$) must be treated separately from the other ($N \geq 2$) cases, since the length of a blinking event cannot be negative. With an activation length R, the probability of the blinking event captured on a given frame number is

$$P_1 = \int_0^R \frac{1}{R} \int_0^{T-t_s} \frac{1}{\tau} e^{-t_l/\tau} dt_l dt_s, \tag{2a}$$

$$P_N = \int_0^R \frac{1}{R} \int_{(N-1)T-t_s}^{NT-t_s} \frac{1}{\tau} e^{-t_l/\tau} dt_l dt_s. \tag{2b}$$
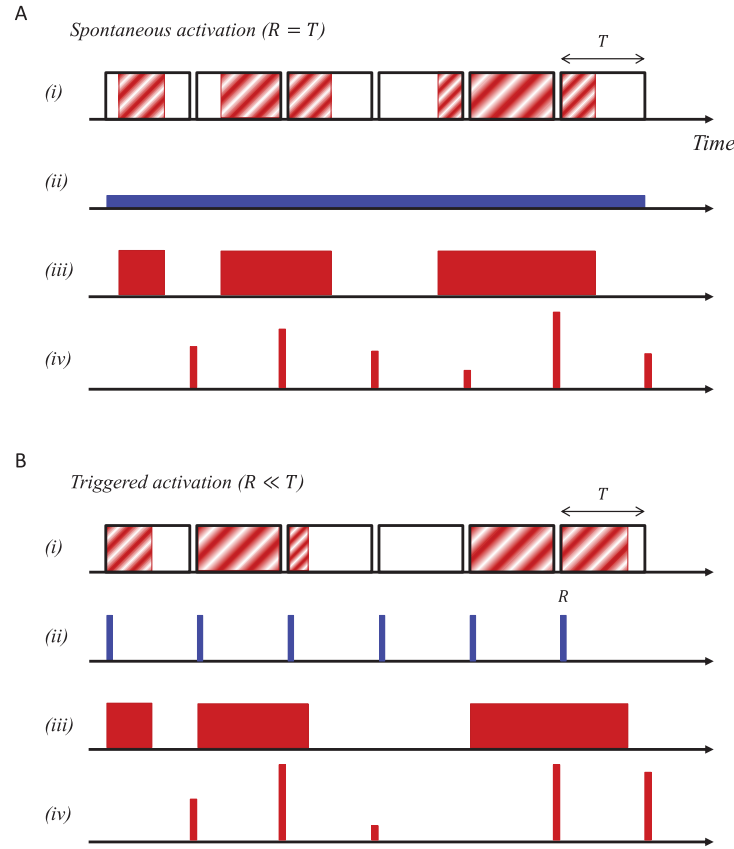
Fig. 1. Concepts of the spontaneous (A) and the triggered (B) activation approach. (i) exposure, (ii) UV activation, (iii) fluorescence, (iv) detected signal after one camera frame integration. Instead of continuous activation (where the activation time on a single frame (R) equals the exposure time (T), activation is achieved with short illumination periods, making the blinking events start at the beginning of an exposure.

Evaluating the integrals, the probabilities are

$$P_1 = 1 - \frac{\tau}{R} \cdot \left(e^{\frac{R-T}{\tau}} - e^{-\frac{T}{\tau}} \right) \tag{3a}$$

$$P_N = \frac{\tau}{R} \cdot \left(e^{\frac{R-(N-1)T}{\tau}} - e^{-\frac{(N-1)T}{\tau}} - e^{\frac{R-NT}{\tau}} + e^{-\frac{NT}{\tau}} \right), \tag{3b}$$

where $R = T$ means spontaneous reactivation, and $R \to 0$ describes triggered reactivation. Let K be the ratio of the expected ON-lifetime to the exposure time ($K = \tau/T$). The probabilities for the two activation types are

$$P_1^{SP} = 1 - K + Ke^{-\frac{1}{K}} \tag{4a}$$

$$P_N^{SP} = K \left(e^{-\frac{N-2}{K}} - 2e^{-\frac{N-1}{K}} + e^{-\frac{N}{K}} \right) = Ke^{-\frac{N}{K}} \left(e^{\frac{2}{K}} - 2e^{\frac{1}{K}} + 1 \right) \tag{4b}$$

$$P_1^{TR} = 1 - e^{-\frac{1}{K}} \tag{4c}$$

$$P_N^{TR} = e^{-\frac{N-1}{K}} - e^{-\frac{N}{K}}. \tag{4d}$$

The calculated probability distributions for $K = 0.5$, 1 and 2 are shown in Fig. 2 (for higher K cases, see the Supplement 1 Fig. S1). The probability distribution function for spontaneous

activation follows a single exponential distribution with the exception of the single frame case, which can deviate significantly and can even make the two-frame probability the most likely (for $K > 0.86$). In contrast, triggered activation results in a pure exponential distribution, and the frame duration probabilities can be derived from the cumulative distribution function ($F_N = 1 - e^{-(NT/\tau)}$). In this case, the one-frame probability will always be the most likely, with a higher probability for smaller K values – compared to the two-frame probability (P_1^{TR}/P_2^{TR}), it is 7.39, 2.72 and 1.65 times more likely (for $K = 0.5$, 1 and 2, respectively). However, reducing the value of K (increasing the exposure time) also significantly increases the measurement time (and the overlapping probability), which should also be taken into consideration. As K approaches infinity, the limit of the ratio of the single frame probabilities (P_1^{TR}/P_1^{SP}) is 2, although both probabilities tend to zero.
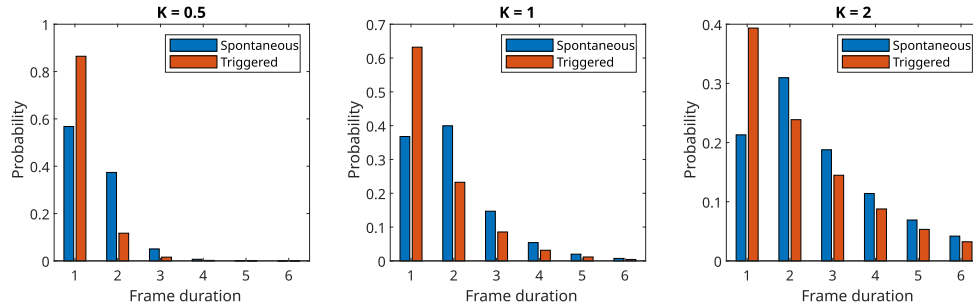

Fig. 2. Frame duration probabilities for $K = 0.5$, 1 and 2.

2.1.2. Average frame number

Knowing the frame duration probabilities, the average number of frames that capture the blinking event ($\overline{N} = \sum_{N=1}^{\infty} N \cdot P_N$) can be calculated. These average frame numbers for the two activation methods are plotted in Fig. 3(A), showing a decrease for the triggered one. This means the emitted photons are captured on fewer frames on average.

The $K = 1$ case is particularly significant, as in practice the exposure time is usually matched to the expected ON-time. In this case, the average frame number is 2 for a spontaneous blinking event (as expected [14]), and 1.582 for a triggered one, which is a 20.9% relative change. We also used $K = 1$ to calculate the overlapping probability and the average time durations.

2.1.3. Overlapping probability

Blinking events captured on fewer frames on average also decrease the probability of overlapping localizations. The overlapping probabilities for a given blinking density can be determined on the basis of the frame duration distributions. Let us choose a blinking event localized on N frames. The number of blinking events within a given time interval and region follows the Poisson distribution, which means that the probability that no other blinking event will occur during the examined N frames is

$$\mathcal{P}_0(N, \rho_0) = e^{-\rho_0 \tau} e^{-\rho_0 NT}, \tag{5}$$

where ρ_0 is the temporal density of blinking events within a diffraction-limited spot. We note that ρ_0 can be expressed with the commonly used duty cycle: $\rho_0 \tau = Dn$, where D is the duty cycle and n is the number of fluorophores within a diffraction limited spot. More stringent restrictions can be applied, for example by recording a signal-free frame before and after the examined N frames to completely separate the blinking event from others. This can make the grouping of
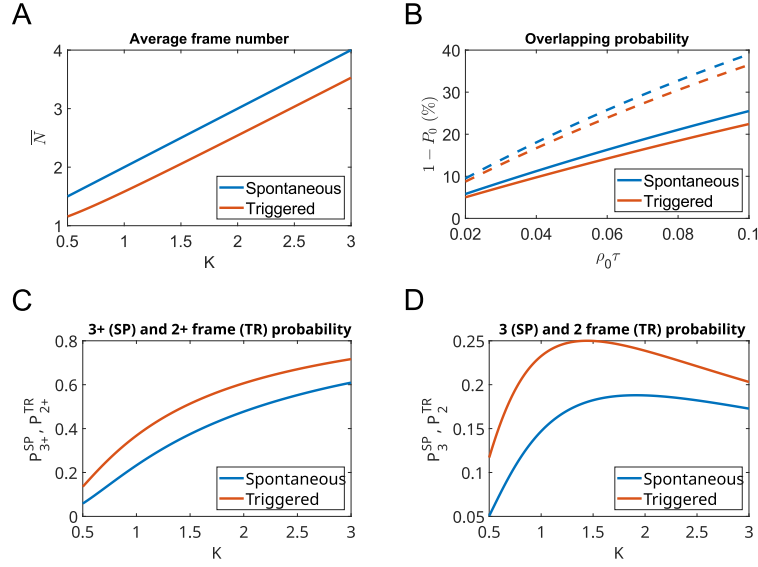
Fig. 3. Average frame number (A), overlapping probability for $t_b = 0$ (solid) and for $t_b = 2T$ (dashed) (B), the probability of capturing the blinking event during an entire exposure (C) and the three- and two-frame probabilities (D).

localizations unambiguous and be useful for background determination [36]. This blank time ($t_b = 2T$) is added to the NT in the exponential, leading to the following equation:

$$\mathcal{P}_0\left(N, \rho_0\right) = e^{-\rho_0\tau} e^{-\rho_0(N+2)T}. \tag{6}$$

To get rid of the dependence on the arbitrarily chosen, examined blinking event frame duration, we must consider the different frame duration probabilities of the trajectories:

$$\mathcal{P}_0\left(\rho_0\right) = \frac{\sum_{N=1}^{\infty} \mathcal{P}_0\left(N, \rho_0\right) P_N}{\sum_{N=1}^{\infty} P_N}. \tag{7}$$

Substituting the calculated probability distributions for $K = 1$, the probability that blinking events will not overlap is

$$\mathcal{P}_0^{SP}\left(\rho_0\right) = e^{-2\rho_0\tau-1} e^{-\rho_0 t_b} \left(1 + \frac{e^2 - 2e + 1}{e^{\rho_0\tau+1} - 1}\right) \tag{8a}$$

$$\mathcal{P}_0^{TR}\left(\rho_0\right) = e^{-\rho_0\tau} e^{-\rho_0 t_b} \left(\frac{e - 1}{e^{\rho_0\tau+1} - 1}\right), \tag{8b}$$

where $t_b = 0$ describes the unrestricted case and $t_b = 2T$ describes the more restricted one. The calculated overlapping probability for spontaneous and triggered activation as a function of the temporal density is shown in Fig. 3(B) ($t_b = 0$: solid, $t_b = 2T$: dashed). The relative change is about 12.8% for $t_b = 0$ and 7.2% for $t_b = 2T$. The derived general formulas for any given K value can be seen in the Supplement 1 Eq. S20a and Eq. S20b.

2.1.4. Average time durations

Blinking events captured on fewer frames on average means they spend more time on these affected frames which increases the intensity of the detected PSF. The average time duration of

blinking events captured on a given frame number can be calculated in a similar way to the frame number probabilities (Eq. (2a,2b)):

$$\mathcal{T}_1 = \frac{\int_0^R \frac{1}{R} \int_0^{T-t_s} \frac{1}{\tau} e^{-t_l/\tau} t_l \, dt_l \, dt_s}{\int_0^R \frac{1}{R} \int_0^{T-t_s} \frac{1}{\tau} e^{-t_l/\tau} \, dt_l \, dt_s} \tag{9a}$$

$$\mathcal{T}_N = \frac{\int_0^R \frac{1}{R} \int_{(N-1)T-t_s}^{NT-t_s} \frac{1}{\tau} e^{-t_l/\tau} t_l \, dt_l \, dt_s}{\int_0^R \frac{1}{R} \int_{(N-1)T-t_s}^{NT-t_s} \frac{1}{\tau} e^{-t_l/\tau} \, dt_l \, dt_s}. \tag{9b}$$

Evaluating the integrals for $K = 1$, the general expressions are

$$\mathcal{T}_1^{SP} = T \cdot \frac{\frac{3}{e} - 1}{\frac{1}{e}} \tag{10a}$$

$$\mathcal{T}_N^{SP} = T \cdot \frac{\frac{N}{e^{N-2}} - \frac{2(N+1)}{e^{N-1}} + \frac{N+2}{e^N}}{\frac{1}{e^{N-2}} - \frac{2}{e^{N-1}} + \frac{1}{e^N}} \tag{10b}$$

$$\mathcal{T}_1^{TR} = T \cdot \frac{1 - \frac{2}{e}}{1 - \frac{1}{e}} \tag{10c}$$

$$\mathcal{T}_N^{TR} = T \cdot \frac{\frac{N}{e^{N-1}} - \frac{N+1}{e^N}}{\frac{1}{e^{N-1}} - \frac{1}{e^N}}. \tag{10d}$$

These average durations are 0.282, 0.836, 1.836, ... for spontaneous activation and 0.418, 1.418, 2.418, ... for triggered activation in T units for $N = 1, 2, 3, \ldots$ respectively ($K = 1$). This means the intensity of the PSF increases by 48% for blinking events that are captured on a single frame. For three or more frame durations, the middle frames always capture the blinking event from the beginning of the frame to the end of it, increasing the average durations by one.

2.1.5. Blinking event's brightness

The brightness of the blinking events (emitted photons over time) carries useful information about the local excitation level, which is often used for local excitation intensity mapping [37–41] or even for determining axial position [42]. This requires a frame that captures the blinking event during the entire exposure [43], which necessitates at least three consecutive frames for spontaneous activation or at least two frames for triggered activation. Decreasing the exposure time to oversample the fluorescent ON time increases the probability of capturing such frames ($P_{3+} = \sum_{i=3}^{\infty} P_i$ for at least three consecutive frames, $P_{2+} = \sum_{i=2}^{\infty} P_i$ for at least two consecutive frames) as it is shown in Fig. 3(C), but it also reduces the precision of these localizations. One can maximize the three-frame probability for spontaneous activation and the two-frame probability for triggered activation in order to retain high photon count localizations (and keep the data size low). Figure 3(D) shows the three- and two-frame probabilities as a function of K, indicating an ideal ON time / frame time ratio (K) of 1.91 for spontaneous activation, and 1.44 for the triggered activation (this means that less oversampling is required for brightness determination for the triggered activation).

2.2. TestSTORM simulations

Calculations give a statistical analysis of the molecule blinking events. In order to analyze the effects of triggered activation on the localization data and the reconstructed image, we generated simulated image stacks for both spontaneous and triggered activation with TestSTORM.
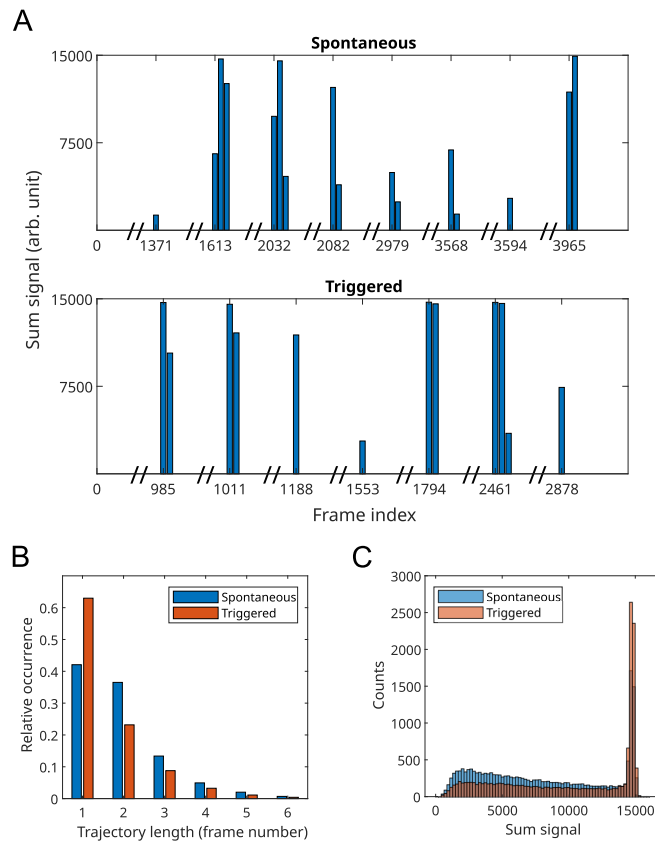
Fig. 4. Sum signal of a selected area as a function of time (axis breaks are represented by two lines) (A), fitted trajectory length histograms (B) and sum signal histograms (C) of datasets simulated by TestSTORM for spontaneous and triggered activation.

In TestSTORM, dye molecules are modeled by a 3-state system (ON, OFF, bleached), with transitions described by characteristic rate constants. The temporal trajectories for the individual dye molecules are generated, then cut into frames by the exposure time. A modified version of TestSTORM (available on Gitlab [44]) was made for triggered activation by rounding the calculated transition times to be a multiple of the exposure time, making every ON-state start at the beginning of a frame.

First, we ran simulations without geometrical structures (Supplement 1 Fig. S2(A)) for comparison with the calculations. To visualize the two activation approaches, the detected signal of the blinking events is plotted as a function of time in Fig. 4(A), showing ones that start at the middle of an exposure (spontaneous activation) and others that start at the beginning (triggered activation) resulting in a first frame completely filled by the blinking event having a sum signal value of $\sim 15,000$ (small variations are due to simulated photon noises and fitting errors). For the spontaneous and triggered activation we generated image stacks (three for each) with 5,000 frames, which we then localized, filtered and trajectory fitted in RainSTORM [45]. Pattern and dye parameters were the same for all stacks (lattice pattern with default Alexa Fluor 647 dye parameters - Supplement 1 Table S1), and the simulated exposure time was equal to the characteristic rate time of the ON-state (50 ms, $K = 1$ - Supplement 1 Table S2). The trajectory length distributions (Fig. 4(B)) are consistent with the calculated probability distributions (Fig. 2, $K = 1$), and slight deviations may occur due to weak localizations (that spend a short amount of

time on a given frame) filtered out during the localization process. Although the total number of localizations is lower compared to spontaneous activation (57,360 for spontaneous vs 46,852 for triggered), triggered activation results in a higher peak at ∼ 15,000 camera count sum signal value given by localizations which fully fill out an exposure, as can be seen in the sum signal histograms (Fig. 4(C)). The mean value for spontaneous and triggered activation is 8,176 and 9,995 camera counts, respectively. This is also consistent with the calculations, as the average frame number decreases for triggered activation, resulting in fewer localizations overall, but with a higher mean sum signal value and a higher probability of filling out an exposure completely.

Next we generated datasets mimicking real measurements to visualize the differences between the reconstructed images for the two activation approaches. The simulated structure was a double-line pattern (Supplement 1 Fig. S2(B)), which is the structure of several sarcomeric proteins with known dimensions from previous measurements [46]. Simulation parameters were used as described earlier [47]. Briefly, we generated disk patterns with a radius of 750 nm, forming double-line patterns with a distance of 110 nm. The distance between double-line objects were 3.4 *μm*, with labeling parameters (Supplement 1 Table S1) set similarly as in the previous measurements [46]. 30,000 frames were generated containing 6 double-line structures for both spontaneous and triggered activation with an exposure time matching the characteristic rate time of the ON-state (30 ms - Supplement 1 Table S2). The simulated datasets were evaluated the same way as the previous measurements [46]: image stacks were localized and filtered in RainSTORM, then exported areas containing the double-line structures were merged using the IFM Analyzer tool [48], and the longitudinal density distributions were fitted with a double Gaussian model that takes into account the localization precision and the linker length. As the emitted photons are detected in fewer frames, resulting in localizations with higher sum signal values, stricter filters can be applied to reconstruct the final image. Merged images were generated with and without
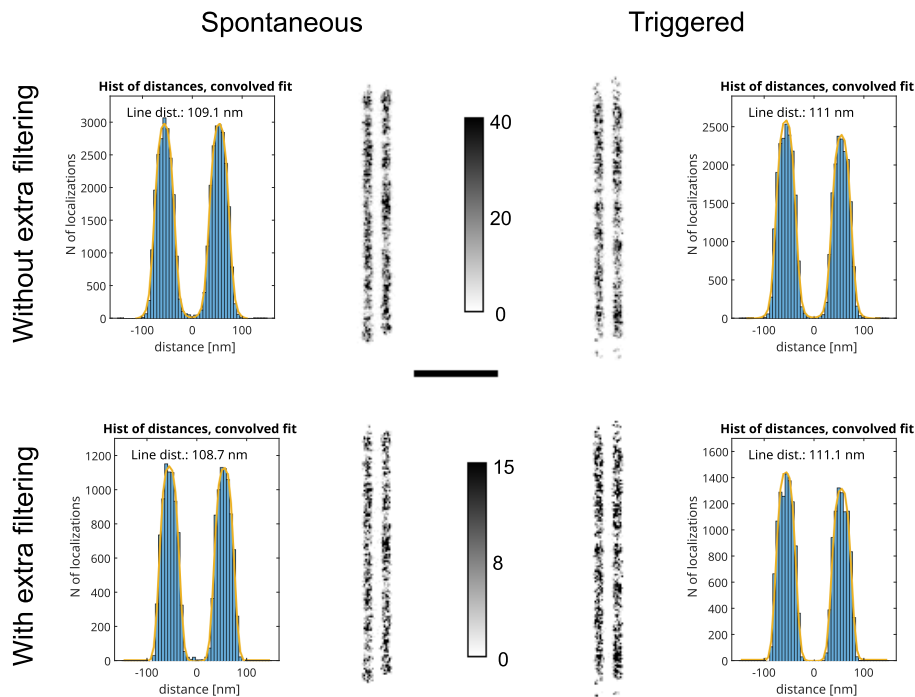

Fig. 5. Merged images and localization histograms (with the fitted double Gaussian models) of the simulated double-line structures with and without extra filtering. Scale bar: 500 nm.

an extra filter eliminating localizations under a sum signal value of 5,000 camera count (Fig. 5). Without this additional filter, spontaneous activation results in more localizations (41010 vs 34163), but after filtering this tendency is reversed (14994 vs 18379). We compared the localized datasets with the ground truth using the distance measure [49,50] to quantify the accuracy of the methods. Without the extra filter, the mean distances are 12.83 nm for spontaneous activation (16.08 nm accuracy) and 8.92 nm for triggered (11.18 nm accuracy). With the extra filter the mean distances changed to 11.02 nm (14.01 nm accuracy) and 6.30 nm (7.90 nm accuracy), respectively.

3.   Preliminary measurements

We performed measurements on a known biological sample published in a previous work [46]. We chose AlexaFluor647 labeled kettin (lg16) protein in the asynchronous indirect flight muscle of Drosophila melanogaster, which forms a double-line structure in the I-band, prepared the same as earlier [51]. Before measurements, samples were reduced for 5 min with aqueous 10 mM NaBH4 (to generate photoactivatable fluorophores by reductive caging) [28], ensuring that the majority of the fluorophores turned into a stable OFF state. We assume negligible thermal/excitation-induced activation compared to the UV-induced activation. Those fluorophores that remained in the ON state were bleached prior to the reactivation. The samples were mounted in 1 mM (UV-treated) Trolox + 100 mM Tris (pH 8.0) + GLOX buffer (enzymatic oxygen scavenging system consisting of 0.5 mg/mL glucose oxidase (GLOX), 40 µg/mL catalase and 5% (w/v) glucose) [13]. We used the same experimental setup as previously described [46]. Briefly, a custom-made microscope system was used based on a Nikon Eclipse Ti-E frame with a Nikon objective (CFI Apo 100x, 1.49 NA). Images were captured by an EMCCD camera (Andor iXon3 897) under EPI illumination of a 647 nm laser (MPB Communications). To activate the reduced dye molecules, an additional diode laser was used at an excitation wavelength of 405 nm. The diode current was set by a Thorlabs controller used in either the constant current mode (spontaneous activation) or with the current modulated with a signal generator (triggered activation). The signal generator was triggered by the rising edge of the camera's FIRE output, sending a square signal (with a width of 5 ms) to the controller at the beginning of each exposure. From each region of interest, 10,000 frames were acquired with an exposure time of 100 ms and an excitation power of 300 mW ($\sim 5kW/cm^2$ at 647 nm excitation). Image stacks containing over 65 double-line structures for both activation methods were localized and filtered with RainSTORM.

Spontaneous activation results in more localizations per double-line (6,650 vs 6,300) compared to triggered activation, while the mean sum signal for the latter increases (4,120 vs 4,700). As shown in the simulations, the number of localizations with low sum signal decreases (under 4,500 sum signal value, 325,000 vs 292,000), while an increase can be observed at the higher values (over 4,500 sum signal value, 121,000 vs 156,000). Based on this, merged images and localization histograms were generated with and without an extra filter eliminating localizations under a sum signal value of 4,500 (Fig. 6), similar to the simulations (Fig. 5). The measured contrast value on the merged histograms is higher for triggered activation (76.16%), which increases further after this additional filter (86.98%) and hence the image contrast improves by 33%. We used the distance measure to quantify the precision of the methods. We calculated the pairwise distances between the double-line structures and used the average of the mean distances to determine the precision. Without the extra filter the average values are 45.72 nm for spontaneous (57.30 nm precision) and 39.32 nm for triggered activation (49.28 nm precision). With the extra filter these values are 47.02 nm for spontaneous (58.92 nm precision) and 44.22 nm for triggered activation (55.42 nm precision). After filtering, the localization density decreases, so the average distance between localizations increases resulting in higher precision values.
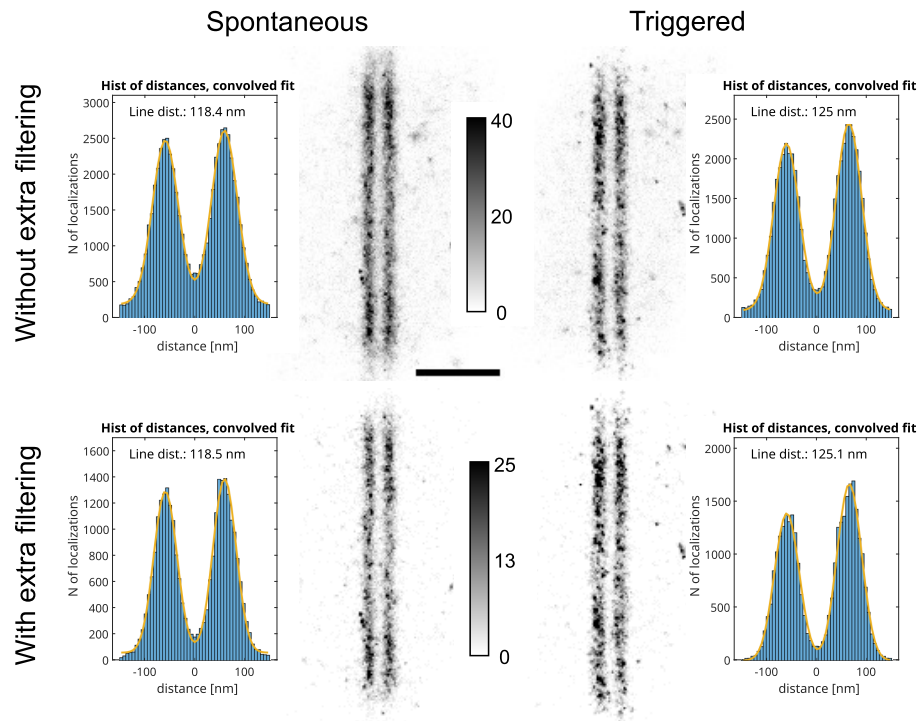
Fig. 6. Merged images and localization histograms (with the fitted double Gaussian models) of the measured double-line structures with and without extra filtering. Scale bar: 500 nm.

4. Discussion

In this work we compared the spontaneous and triggered activation approach, which applies to all photoactivatable fluorophores such as caged dyes and photoactivatable/photoconvertible fluorescent proteins. Based on a statistical model, we calculated the frame duration probabilities, which follow a single exponential distribution with the exception of the spontaneous single frame probability. This leads to a decrease in the average frame number for the triggered case, meaning that the blinking events (the emitted photons) are captured on fewer frames on average, resulting in fewer but higher photon number localizations. The lower average frame number also decreases the probability of overlaps (by 7 to 13%). The triggered approach is also advantageous in determining the blinking events' intensity and position, since less oversampling is required. We used TestSTORM simulations to show these differences on 2D images. This showed that the total number of localizations decreases with the triggered activation, but the mean sum signal value increases by 20%. This is caused by the increase in localizations with higher sum signal values, allowing stricter filters for the localization data. We also performed measurements on biological samples, showing this increase in the sum signal values, and the effect of this additional filter on the merged images.

Disclosures. The authors declare no conflicts of interest.

Data availability. Data underlying the results presented in this paper are not publicly available at this time but may be obtained from the authors upon reasonable request.

Supplemental document. See Supplement 1 for supporting content.

References

1. M. G. Gustafsson, "Surpassing the lateral resolution limit by a factor of two using structured illumination microscopy," J. Microsc. **198**(2), 82–87 (2000).
2. S. W. Hell and J. Wichmann, "Breaking the diffraction resolution limit by stimulated emission: stimulated-emission-depletion fluorescence microscopy," Opt. Lett. **19**(11), 780–782 (1994).
3. M. Lelek, M. T. Gyparaki, and G. Beliu, "Single-molecule localization microscopy," Nat. Rev. Methods Primers **1**(1), 39 (2021).
4. E. Betzig, G. H. Patterson, and R. Sougrat, "Imaging intracellular fluorescent proteins at nanometer resolution," Science **313**(5793), 1642–1645 (2006).
5. S. T. Hess, T. P. Girirajan, and M. D. Mason, "Ultra-high resolution imaging by fluorescence photoactivation localization microscopy," Biophys. J. **91**(11), 4258–4272 (2006).
6. M. J. Rust, M. Bates, and X. Zhuang, "Sub-diffraction-limit imaging by stochastic optical reconstruction microscopy (storm)," Nat. Methods **3**(10), 793–796 (2006).
7. M. Heilemann, S. Van De Linde, and M. Schüttpelz, "Subdiffraction-resolution fluorescence imaging with conventional fluorescent probes," Angew. Chem., Int. Ed. **47**(33), 6172–6176 (2008).
8. A. Sharonov and R. M. Hochstrasser, "Wide-field subdiffraction imaging by accumulated binding of diffusing probes," Proc. Natl. Acad. Sci. **103**(50), 18911–18916 (2006).
9. J. Fölling, M. Bossi, and H. Bock, "Fluorescence nanoscopy by ground-state depletion and single-molecule return," Nat. Methods **5**(11), 943–945 (2008).
10. F. Balzarotti, Y. Eilers, and K. C. Gwosch, "Nanometer resolution imaging and tracking of fluorescent molecules with minimal photon fluxes," Science **355**(6325), 606–612 (2017).
11. M. Sauer, "Localization microscopy coming of age: from concepts to biological impact," J. Cell Sci. **126**(16), 3505–3513 (2013).
12. R. E. Thompson, D. R. Larson, and W. W. Webb, "Precise nanometer localization analysis for individual fluorescent probes," Biophys. J. **82**(5), 2775–2783 (2002).
13. S. Van de Linde, A. Löschberger, and T. Klein, "Direct stochastic optical reconstruction microscopy with standard fluorescent probes," Nat. Protoc. **6**(7), 991–1009 (2011).
14. U. Endesfelder, S. Malkusch, F. Fricke, *et al.*, "A simple method to estimate the average localization precision of a single-molecule localization microscopy experiment," Histochem. Cell Biol. **141**(6), 629–638 (2014).
15. W. Vandenberg, M. Leutenegger, and T. Lasser, "Diffraction-unlimited imaging: from pretty pictures to hard numbers," Cell Tissue Res. **360**(1), 151–178 (2015).
16. F. Fricke, M. S. Dietz, and M. Heilemann, "Single-molecule methods to study membrane receptor oligomerization," ChemPhysChem **16**(4), 713–721 (2015).
17. E. M. Puchner, J. M. Walter, and R. Kasper, "Counting molecules in single organelles with superresolution microscopy allows tracking of the endosome maturation trajectory," Proc. Natl. Acad. Sci. **110**(40), 16015–16020 (2013).
18. X. Nan, E. A. Collisson, and S. Lewis, "Single-molecule superresolution imaging allows quantitative analysis of raf multimer formation and signaling," Proc. Natl. Acad. Sci. **110**(46), 18519–18524 (2013).
19. P. Annibale, S. Vanni, and M. Scarselli, "Quantitative photo activated localization microscopy: unraveling the effects of photoblinking," PLoS One **6**(7), e22678 (2011).
20. S.-H. Lee, J. Y. Shin, A. Lee, *et al.*, "Counting single photoactivatable fluorescent molecules by photoactivated localization microscopy (palm)," Proc. Natl. Acad. Sci. **109**(43), 17436–17441 (2012).
21. M. Bates, S. A. Jones, and X. Zhuang, "Stochastic optical reconstruction microscopy (STORM): a method for superresolution fluorescence imaging," Cold Spring Harbor Protocols **2013**(6), pdb.top075143 (2013).
22. M. Sun, J. Huang, and F. Bunyak, "Superresolution microscope image reconstruction by spatiotemporal object decomposition and association: application in resolving t-tubule structure in skeletal muscle," Opt. Express **22**(10), 12160–12176 (2014).
23. K. J. Martens, B. Turkowyd, and U. Endesfelder, "Raw data to results: a hands-on introduction and overview of computational analysis for single-molecule localization microscopy," Front. Bioinform. **1**, 817254 (2022).
24. T. Cordes, M. Strackharn, and S. W. Stahl, "Resolving single-molecule assembled patterns with superresolution blink-microscopy," Nano Lett. **10**(2), 645–651 (2010).
25. G. T. Dempsey, J. C. Vaughan, and K. H. Chen, "Evaluation of fluorophores for optimal performance in localization-based super-resolution imaging," Nat. Methods **8**(12), 1027–1036 (2011).
26. L. Herdly, P. W. Tinning, and A. Geiser, "Benchmarking thiolate-driven photoswitching of cyanine dyes," J. Phys. Chem. B **127**(3), 732–741 (2023).
27. H. Shroff, C. G. Galbraith, J. A. Galbraith, *et al.*, "Live-cell photoactivated localization microscopy of nanoscale adhesion dynamics," Nat. Methods **5**(5), 417–423 (2008).
28. J. C. Vaughan, S. Jia, and X. Zhuang, "Ultrabright photoactivatable fluorophores created by reductive caging," Nat. Methods **9**(12), 1181–1184 (2012).
29. S. Jang, M. Kim, and S.-H. Shim, "Reductively caged, photoactivatable dna-paint for high-throughput super-resolution microscopy," Angew. Chem., Int. Ed. **59**(29), 11758–11762 (2020).

30. M. Lehmann, B. Gottschalk, and D. Puchkov, "Multicolor caged dstorm resolves the ultrastructure of synaptic vesicles in the brain," Angew. Chem. **127**(45), 13428–13433 (2015).

31. L. Carlini, A. Benke, and L. Reymond, "Reduced dyes enhance single-molecule localization density for live superresolution imaging," ChemPhysChem **15**(4), 750–755 (2014).

32. M. Bates, B. Huang, G. T. Dempsey, *et al.*, "Multicolor super-resolution imaging with photo-switchable fluorescent probes," Science **317**(5845), 1749–1753 (2007).

33. A. Dani, B. Huang, and J. Bergan, "Superresolution imaging of chemical synapses in the brain," Neuron **68**(5), 843–856 (2010).

34. J. Sinkó, R. Kákonyi, and E. Rees, "Teststorm: Simulator for optimizing sample labeling and image acquisition in localization based super-resolution microscopy," Biomed. Opt. Express **5**(3), 778–787 (2014).

35. T. Novák, T. Gajdos, and J. Sinkó, "Teststorm: Versatile simulator software for multimodal super-resolution localization fluorescence microscopy," Sci. Rep. **7**(1), 951 (2017).

36. B. P. Isaacoff, Y. Li, S. A. Lee, *et al.*, "Small-labs: Measuring single-molecule intensity and position in obscuring backgrounds," Biophys. J. **116**(6), 975–982 (2019).

37. C. Steuwe, M. Erdelyi, and G. Szekeres, "Visualizing electromagnetic fields at the nanoscale by single molecule localization," Nano Lett. **15**(5), 3217–3223 (2015).

38. B. Fu, J. D. Flynn, and B. P. Isaacoff, "Super-resolving the distance-dependent plasmon-enhanced fluorescence of single dye and fluorescent protein molecules," J. Phys. Chem. C **119**(33), 19350–19358 (2015).

39. E. Johlin, J. Solari, and S. A. Mann, "Super-resolution imaging of light-matter interactions near single semiconductor nanowires," Nat. Commun. **7**(1), 13950 (2016).

40. D. L. Mack, E. Cortés, and V. Giannini, "Decoupling absorption and emission processes in super-resolution localization of emitters in a plasmonic hotspot," Nat. Commun. **8**(1), 14513 (2017).

41. E. Tóth, D. Ungor, and T. Novák, "Mapping fluorescence enhancement of plasmonic nanorod coupled dye molecules," Nanomaterials **10**(6), 1048 (2020).

42. A. M. Szalai, B. Siarry, and J. Lukin, "Three-dimensional total-internal reflection fluorescence nanoscopy with nanometric axial resolution by photometric localization of single molecules," Nat. Commun. **12**(1), 517 (2021).

43. Y. Shen, T. He, and W. Wang, "Fluorescence enhancement on silver nanoplates at the single-and sub-nanoparticle level," Nanoscale **7**(47), 20132–20141 (2015).

44. P. Bíró, "TestSTORM modified," Gitlab, 2024, https://gitlab.com/adoptim/testSTORM/-/tree/cage.

45. E. J. Rees, M. Erdelyi, and G. S. K. Schierle, "Elements of image processing in localization microscopy," J. Opt. **15**(9), 094012 (2013).

46. S. Szikora, T. Gajdos, and T. Novák, "Nanoscopy reveals the layered organization of the sarcomeric h-zone and i-band complexes," J. Cell Biol. **219**(1), e201907026 (2020).

47. D. Varga, S. Szikora, and T. Novák, "Machine learning framework to segment sarcomeric structures in smlm data," Sci. Rep. **13**(1), 1582 (2023).

48. Advanced Optical Imaging Group, "IFM Analyzer," University of Szeged, 2024, https://titan.physx.u-szeged.hu/~adoptim/?page_id=1246.

49. G. D. B. Vazquez, S. Martínez, and O. E. Martínez, "Super-resolved edge detection in optical microscopy images by superposition of virtual point sources," Opt. Express **28**(17), 25319–25334 (2020).

50. M. Toscani, O. E. Martínez, and S. Martínez, "Resolution, accuracy and precision in super-resolved microscopy images using suppose," Optics and Lasers in Engineering **161**, 107337 (2023).

51. S. Szikora, T. Novák, and T. Gajdos, "Superresolution microscopy of drosophila indirect flight muscle sarcomeres," Bio-Protoc. **10**(12), e3654 (2020).